Journal of Medicinal Chemistry

Article

pubs.acs.org/jmc

Astemizole Arrests the Proliferation of Cancer Cells by Disrupting the EZH2-EED Interaction of Polycomb Repressive Complex 2

Xiangqian Kong,[†,‡] Limin Chen,[†,‡] Lianying Jiao,[§] Xiangrui Jiang,[†] Fulin Lian,[†] Junyan Lu,[†] Kongkai Zhu,[†] Daohai Du,[†] Jingqiu Liu,[†] Hong Ding,[†] Naixia Zhang,[†] Jingshan Shen,[†] Mingyue Zheng,[†] Kaixian Chen,[†] Xin Liu,[§] Hualiang Jiang,[†] and Cheng Luo*[,†]

[†]State Key Laboratory of Drug Research, Shanghai Institute of Materia Medica, Chinese Academy of Sciences, Shanghai 201203 P. R. China

[§]Cecil H. and Ida Green Center for Reproductive Biology Sciences, UT Southwestern Medical Center, Dallas, Texas 75390, United States

Supporting Information

ABSTRACT: Polycomb Repressive Complex 2 (PRC2) modulates the chromatin structure and transcriptional repression by trimethylation lysine 27 of histone H3 (H3K27me3), a process that necessitates the protein−protein interaction (PPI) between the catalytic subunit EZH2 and EED. Deregulated PRC2 is intimately involved in tumorigenesis and progression, making it an invaluable target for epigenetic cancer therapy. However, until now, there have been no reported small molecule compounds targeting the EZH2-EED interactions. In the present study, we identified astemizole, an FDA-approved drug, as a small molecule inhibitor of the EZH2-EED interaction of PRC2. The disruption of the EZH2-EED interaction by astemizole destabilizes the PRC2 complex and inhibits its methyltransferase activity in cancer cells. Multiple lines of evidence have demonstrated that astemizole arrests the proliferation of PRC2-driven lymphomas primarily by disabling the PRC2 complex. Our findings demonstrate the chemical tractability of the difficult PPI target by a small molecule compound, highlighting the therapeutic promise for PRC2-driven human cancers via targeted destruction of the EZH2-EED complex.

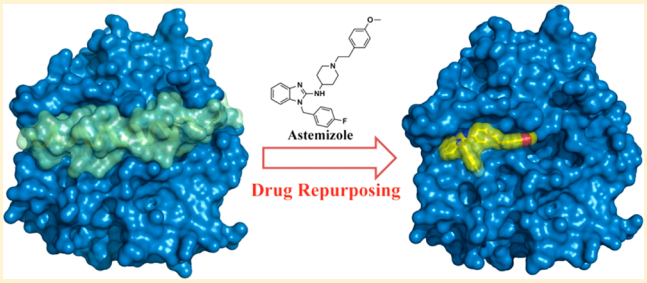

INTRODUCTION

The post-translational modifications of histones, such as methylation, acetylation, phosphorylation, and ubiquitination, orchestrate the gene expression in a spatial and temporal-specific manner by modulating the chromatin structure or recruiting the "Reader" proteins.[1,2] Among them, histone methylation is regarded as one of the most complicated epigenetic modifications because its function relies on the precise methylation sites and the degree of modification.[3−5] A large number of studies have revealed that the elaborate gene regulatory network established by histone methylation is critical for both development and homeostasis.[6] The imbalances between histone methylation and demethylation represent a common indicator for a wide variety of proliferative diseases, especially cancer.[7,8]

The Polycomb group (PcG) proteins are a family of proteins, initially identified in *Drosophila melanogaster*, that are important for early development by regulating the homeotic genes.[9,10] It was subsequently suggested that PcG proteins can remodel chromatin in part through the deposition of histone marks associated with gene repression.[11] In mammals, two major biochemically and functionally distinct multiprotein complexes exist, PRC1 (Polycomb repressive complex 1) and PRC2 (Polycomb repressive complex 2). PRC2 catalyzes the trimethylation of lysine 27 on histone H3 (H3K27me3), a modification that is a hallmark of silent chromatin, and facilitates the recruitment of PRC1 to the specific target loci, indicating that PRC1 functions downstream of PRC2.[12,13] Recent findings highlight the essential role of PRC2 in embryonic development, cell differentiation, and stem-cell plasticity, primarily by catalyzing the H3K27me3.[14−16] The catalytic subunit for depositing the H3K27me3 mark is EZH2, whose activity requires the assembly of a core complex with at least two additional subunits of PRC2, EED, and SUZ12.[17,18] Accumulating data demonstrate that aberrant PRC2 activity has been broadly implicated in cancer initiation and progression.[19] Prevalent overexpression of EZH2 or other PRC2 subunits has been detected in a variety of malignancies and correlates strongly with hyper-trimethylation of H3K27, aggressiveness, and poor prognosis.[20] More recently, recurrent somatic, heterozygous mutations in EZH2 that confer H3K27 hyper-trimethylation have been identified in both GC B-cell type diffuse large B-cell lymphoma (GCB-DLBCL) and follicular

Received: August 10, 2014
Published: November 4, 2014

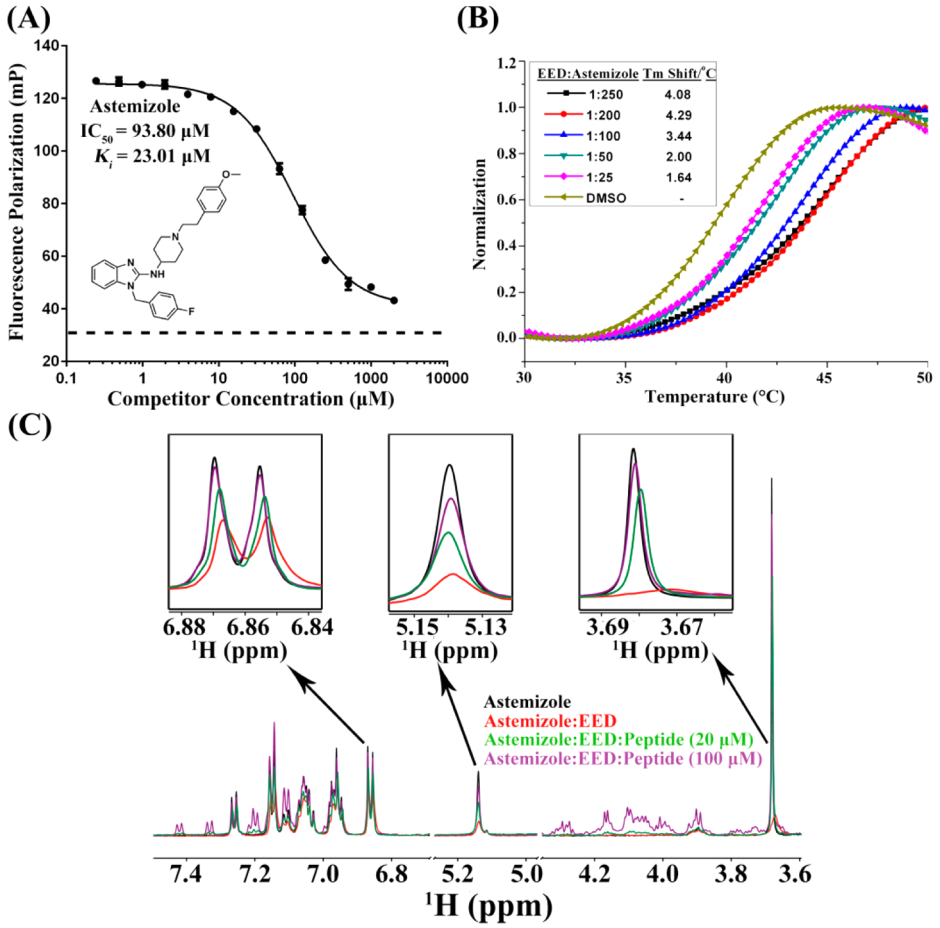

Figure 1. Characterization of astemizole and EED binding. (A) The displacement of FITC-labeled EZH2 peptide by astemizole in the competitive FP assay. The dashed line indicated the background FP value (35 mP) of the free tracer peptide. (B) The thermal shift assay displaying the stabilization of EED by astemizole. (C) T1ρ NMR spectra for astemizole (black), astemizole in the presence of EED (red), and astemizole in the presence of EED and either 20 μM (green) or 100 μM EZH2 peptide (purple).

lymphoma;[21] these mutants, carrying aberrant PRC2 activities, mediate cell differentiation blockade, thus driving certain types of cancer.[22,23] The down-regulation of EZH2 expression by RNA interference (RNAi) suppresses the growth of cancer cells with hyper-activated PRC2 activity.[24] Taken together, these findings strongly suggest that PRC2 is a promising therapeutic target for epigenetic intervention in cancer.

To abrogate the oncogenic potential of EZH2, pyridone-based EZH2 inhibitors have been developed by several pharmaceuticals companies. These inhibitors displayed efficacy in DLBCLs harboring mutated EZH2 or overexpressing wild-type EZH2 in the preclinical studies, validating the causal role of deregulated EZH2 in driving oncogenesis.[24−27] The interaction between EZH2 and EED is required for the integrity and methyltransferase activity of PRC2,[17,28−31] and a recent landmark study demonstrated that a stapled EZH2 peptide selectively inhibits EZH2 activity in cancer cells by disrupting the EZH2-EED complex, destabilizing PRC2.[32] The confirmed druggability of the protein−protein interaction (PPI) between EZH2 and EED may represent a complementary strategy for selectively arresting the proliferation of human cancers, which are addicted to PRC2 activity, unrelated to trimethylation of H3K27, and show limited sensitivity to the EZH2 inhibitors.[32−35] Nevertheless, peptide or peptidomimetic inhibitors largely suffer from poor metabolic stability and low bioavailability, which may hinder their therapeutic application in the clinic.[36,37] Small-molecule PPI modulators with high drug likeness are more amenable from a medicinal chemistry and drug development perspective.[38−42] However, distinct from most druggable protein contacts with relatively narrow binding grooves (average buried surface area (BSA) of approximately 1500 Å^2), the remarkably large interface between EZH2 and EED (nearly 3000 Å^2 of BSA) may introduce special difficulties in developing small-molecule inhibitors because of the slow off-rates and the large surfaces to overcome.[43] To the best of our knowledge, no small-molecule inhibitors have been developed that target the EZH2-EED interaction.

Structure based virtual screening (SBVS) has become a powerful tool in the medicinal chemists' toolkit for rapidly enriching the hits from large pools of virtual compound libraries.[44−47] Herein, we report the identification of astemizole, a previously FDA-approved drug used to treat seasonal allergic rhinitis due to its histamine H1 receptor antagonist activity,[48] as an inhibitor of the EZH2-EED interaction based on a structure-based virtual screening strategy. A combination of biochemical and biophysical characterizations indicate that astemizole may bind to EED in a competitive manner with EZH2. The cell-based studies reveal that astemizole impairs the PRC2 activity via dissociation of the EZH2-EED complex and destabilization of PRC2 complex, inhibiting the proliferation of PRC2-driven lymphomas.

dx.doi.org/10.1021/jm501230c | J. Med. Chem. 2014, 57, 9512−9521

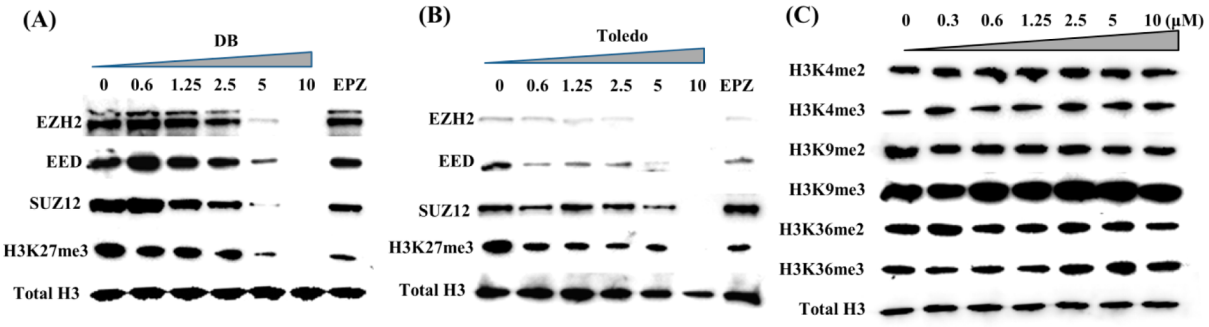

Figure 2. In vivo functional assays for astemizole effects. (A, B) EZH2, EED, and SUZ12 protein and H3K27me3 levels in DB and Toledo cells following treatment with the indicated concentrations of astemizole or 10 μM EPZ. The total histone H3 is shown as a loading control. (C) Western blot against other histone H3 lysine methylation marks using DB cell lysates treated with the indicated concentrations of astemizole. Total histone H3 is shown as a loading control.

RESULTS AND DISCUSSION

Virtual Screening to Identify Astemizole that Disrupts the EZH2-EED Interactions. The crystal structure of EED in complex with EZH2 (Protein Data Bank (PDB) entry: 2QXV)[49] was used as a target for docking-based virtual screening. Residues within 8 Å of F42 in EZH2 were defined as binding sites because of the relatively more "hot-spot" clusters around the N-terminal portion of the EZH2 peptide. An in-house database, containing approximately 1000 known drugs, was screened in silico. The top-100 compounds ranked based on the docking score were retained for visual inspection to remove the compounds with poor shape and chemical fitness with the binding groove as well as with similar chemical scaffolds. Finally, the top-50 compounds were selected for experimental validation. Among them, astemizole, an FDA-approved antiallergy drug with histamine H1 receptor antagonist activity,[48] showed the highest inhibitory activity in a competitive fluorescence polarization (FP) assay (Supporting Information Table S1). It displaced the EZH2 peptide with an inhibition constant (K_i) of 23.01 μM (Figure 1A and Figure S1 in Supporting Information). To determine whether astemizole directly binds to EED and competes with EZH2, we utilized multiple additional methods to characterize the interactions between EED and astemizole. First, a fluorescence-based thermal shift assay indicated that astemizole dose-dependently shifted the melting temperature (T_m) of EED for over 4 °C until reaching a plateau (Figure 1B), suggesting that the EZH2 displacement activity observed in the FP assay was mainly the result of a direct binding event rather than impaired EED thermostability. Next, strong binding signals were clearly observed in both the ligand's observed T1ρ (Figure 1D) and saturation transfer difference (STD) nuclear magnetic resonance (NMR) spectra (Supporting Information Figure S2), and the addition of the EZH2 peptide to the EED-astemizole complex restored the T1ρ effect in a dose-dependent manner, indicating the mutually exclusive binding of astemizole and EZH2 to EED. To investigate the effectiveness of astemizole in inhibiting the enzymatic activity of the PRC2 holoenzyme, an in vitro histone methyltransferase (HMT) assay was used to demonstrate that the HMT activity was inhibited in a dose-dependent manner (Supporting Information Figure S3). Collectively, these biochemical and biophysical results demonstrate the reversible and specific binding of astemizole to EED and confirm that astemizole disrupts the EZH2-EED interaction.

Selective Inhibition of PRC2 Activities by Astemizole in Cells. To explore the ability of astemizole to disable the PRC2 complex in cancer cells, DLBCL cells expressing either wild-type EZH2 (Toledo) or an EZH2 mutant (DB) were exposed to astemizole or a control EZH2 inhibitor, EPZ005687 (EPZ), for 72 h.[25] As indicated in Figure 2A,B, astemizole treatment produced a clear concentration-dependent decrease in the H3K27me3 levels in both the DB and Toledo cell lines. By comparison, the other histone H3 methylation marks were largely unaffected, highlighting the exquisite specificity of astemizole for PRC2 inhibition (Figure 2C). The better activity in inhibiting the PRC2 complex in cells than in vitro suggested that a novel mechanism may be employed by astemizole to inhibit the PRC2 activity. Previous studies emphasized the importance of the EZH2-EED interaction for the integrity of the PRC2 complex, and the dissociation of the EZH2-EED complex by astemizole may thus impair the stability of each PRC2 subunit in vivo. Accordingly, we examined the changes in the protein level of each core component of the PRC2 complex following treatment. As expected, treatment with astemizole dose-dependently depleted the EZH2, EED, and SUZ12 proteins in both cell lines (Figure 2A,B), which is in agreement with the reported effects of mutations that disrupt these protein−protein interactions[30,31] and the effects of the stapled EZH2 peptide.[32] The cell viability, assessed by flow cytometry, indicated that the decrease in the PRC2 protein and H3K27me3 levels may not be attributed to the apoptosis induced by astemizole, especially for the effects observed at lower compound concentrations (Supporting Information Figure S4). By contrast, no such effects were observed for the EZH2 inhibitor EPZ (Figure 2A,B) or the cytotoxic lymphoma chemotherapy drug doxorubicin (Supporting Information Figure S5),[50] emphasizing the distinct mechanism of action (MOA) of astemizole for PRC2 inhibition and eliminating the possibility that the reduction of the PRC2 component and H3K27me3 levels were due to nonspecific cell-growth blocking. Hence, the accelerated degradation of the core components by astemizole led to a more dissociated state of PRC2 complex in cells than in vitro, which may account for its better cellular activity (see Discussion below). Taken together, these results indicate that astemizole selectively suppresses the methyltransferase activity of the PRC2 complex by targeted inhibition of the EZH2-EED interaction, destabilizing the core components of the enzyme complex.

Antiproliferation Activity of Astemizole for the PRC2-Driven DLBCLs. Given that GCB-DLBCL cell growth is

dx.doi.org/10.1021/jm501230c | J. Med. Chem. 2014, 57, 9512−9521

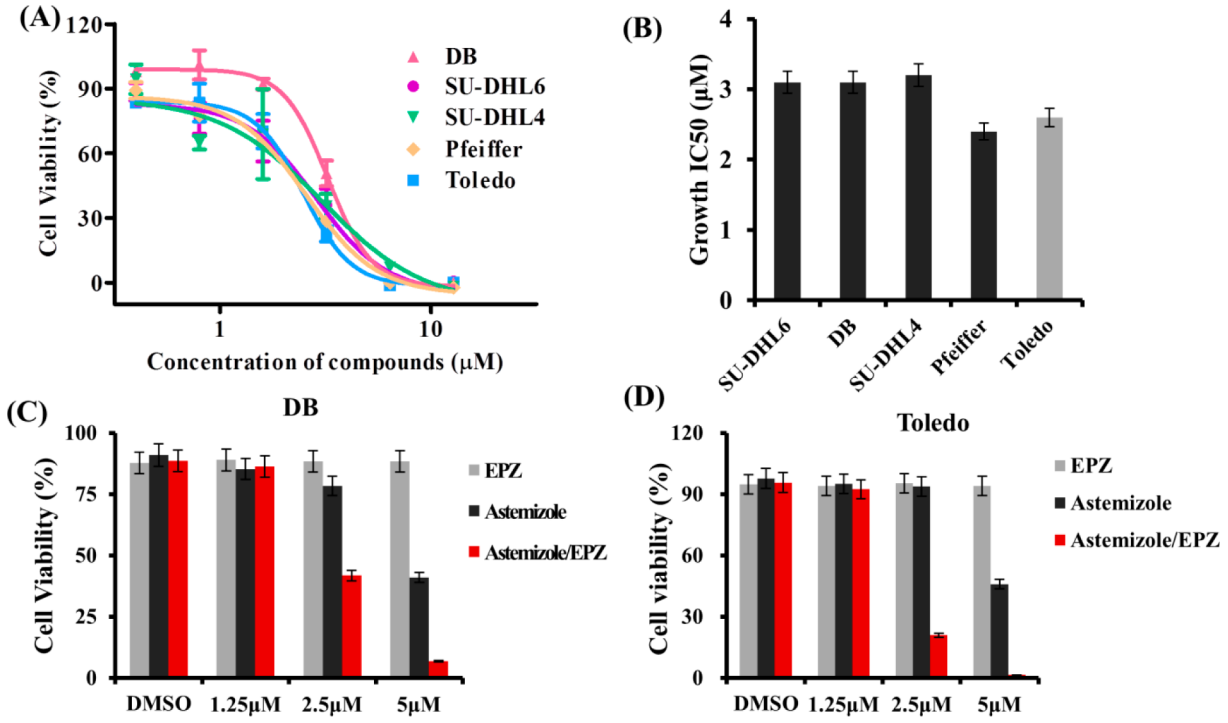

Figure 3. Antiproliferation activity of astemizole for DLBCLs. (A) Cell growth inhibition curves of astemizole for the five GCB-DLBCL cell lines. (B) Effect of astemizole on the growth of DLBCL cell lines represented as the concentration of astemizole required to inhibit 50% of growth (growth IC_{50}). (C, D) Effects of combination treatment at the indicated dose of astemizole and EPZ in DB and Toledo cells. DB and Toledo cells were treated with EPZ and/or astemizole for 72 h, and the cell viability was detected by flow cytometry.

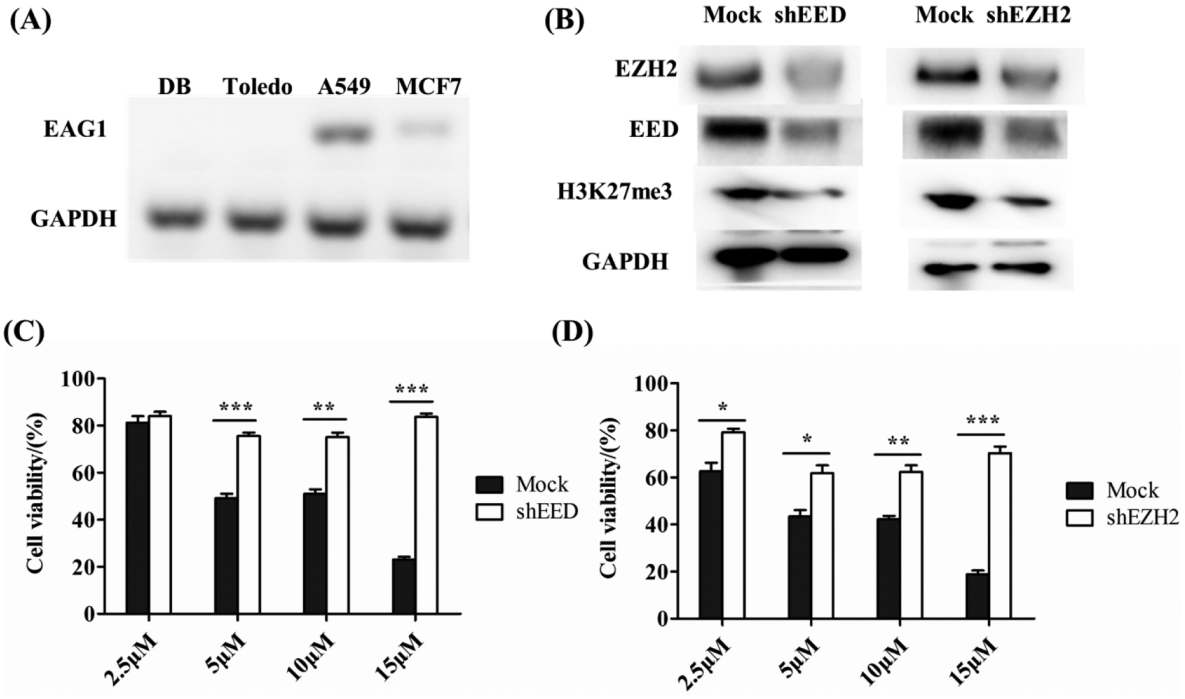

Figure 4. (A) mRNA level of EAG1 in different cancer cell lines. (B) Expression levels of EZH2, EED, and H3K27me3 in mock-treated, shEED-treated, or shEZH2-treated DB cells. (C,D) Antiproliferation activity of astemizole for mock-treated or shEED-treated (C) and shEZH2-treated (D) DB cells. Cell viability was measured by alamar blue after 3 day treatment. * $P < 0.05$, ** $P < 0.01$, *** $P < 0.001$.

driven by aberrant PRC2 activity,[24] we monitored the impact of the intracellular inhibition of PRC2 by astemizole on the viability in these cancer cells. As shown in Figure 3A,B, low micromolar concentrations of astemizole dramatically inhibited the proliferation of GCB-DLBCL cells carrying mutant forms of EZH2 (DB, SU-DHL6, SU-DHL4, and Pfeiffer) or wild-type EZH2 (Toledo), corroborating the essential role of PRC2 in unrestrained cell proliferation.[32] Because the MOAs by which astemizole and EPZ target PRC2 differ, combined treatment with both compounds might yield an enhanced antiprolifera-

dx.doi.org/10.1021/jm501230c | J. Med. Chem. 2014, 57, 9512−9521

tion effect compared with either agent alone. Encouragingly, a prominent synergistic effect was observed in both DB and Toledo cells with the simultaneous administration of astemizole and EPZ (Figure 3C,D), which is consistent with the results for the stapled EZH2 peptide in a recent study.[32] Nearly complete abrogation of cell growth was achieved when a combined dose of 5 μM astemizole and 5 μM EPZ was used. Therefore, our data confirmed that the targeted disruption of the EZH2-EED complex and depletion of the PRC2 core components by astemizole resulted in a therapeutic benefit for GCB-DLBCLs, which can be further strengthened by combination treatment with an EZH2 inhibitor.

Antiproliferation Activity of Astemizole for Lymphomas Was Largely Attributed to the Disruption of the PRC2 Complex. Previous studies suggested that astemizole decreased the proliferation of tumor cells by blocking the *ether à-go-go 1* (EAG1) potassium channel.[51,52] To examine the role of blocking EAG1 in astemizole-induced cell growth arrest for the PRC2-driven lymphomas, we carefully examined the expression level of EAG1 in both DB and Toledo cells by semiquantitative RT-PCR. As shown in Figure 4A, the expression of EAG1 was not detected in either of the two lymphoma cell lines. However, it should be noted that, consistent with other studies, EAG1 can readily be detected in both the lung cancer cell line A549[53,54] and breast cancer cell line MCF7,[55,56] indicating the reliability of the assay. Therefore, our data established that the cell growth arresting effects of astemizole for PRC2-driven lymphomas might be not due to the blockage of the EAG1 ion channel. Furthermore, to investigate the specificity of astemizole for the PRC2 complex in cancer cells, we first established the EZH2 or EED low-expressed cell lines by treating the DB cells with shRNA-specific for EZH2 (shEZH2) or EED (shEED). The simultaneous decrease in the protein level of EED (or EZH2) after knockdown of EHZ2 (or EED) was consistent with the notion that that the disruption of the EZH2-EED complex may impair the stability of the PRC2 core components,[28,30,31] which is in agreement with the effects observed for astemizole as well as the stapled EZH2 peptide (Figure 4B).[32] Then, we compared the differences of the inhibitory activity of astemizole toward the shRNA-treated or mock-treated DB cells. It is evident that the DB cancer cells with low expression of EZH2 or EED were more resistant to the antiproliferation activity of astemizole than the mock-treated cells (Figure 4C,D), especially at higher compound concentrations, indicating that the antiproliferation effects of astemizole may be directly related to the PRC2 complex. Collectively, our data indicated that astemizole inhibits the unrestrained proliferation of lymphoma cells primarily by disabling the PRC2 complex.

Molecular Modeling Studies. To understand the molecular basis of the inhibition of the EZH2-EED interaction, a molecular docking simulation was performed to scrutinize the binding mode of astemizole. In the docking simulation, astemizole was predicted to bind at the sites that overlap with the binding surface of the N-terminal EZH2 peptide on EED (Supporting Information Figure S6).[49] The benzimidazole moiety of astemizole is tightly confined within a cleft that is occupied by the hot-spot residue F42 in EZH2 in the protein complex[49] through extensive hydrophobic interactions with the surrounding residues (Figure 5). Moreover, two hydrogen bonds were formed between 4-aminopiperidine and the carbonyl oxygens of L391 and Q374, and extensive van der

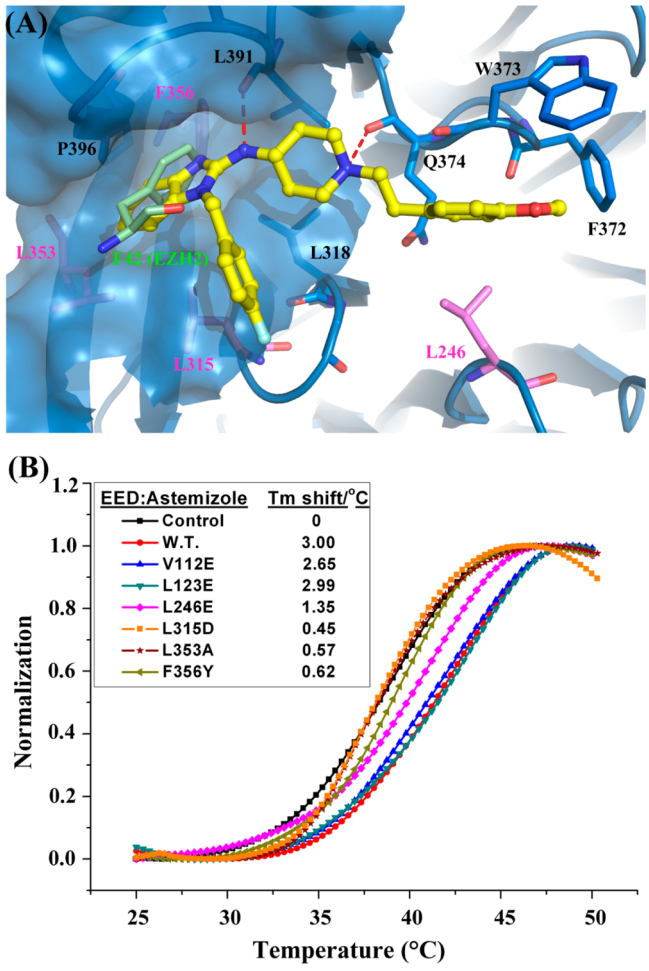

Figure 5. Molecular modeling of the astemizole/EED complex. (A) Detailed interactions between astemizole (yellow sticks) and its surrounding residues in EED (blue or pink sticks). Residues selected for mutagenesis are colored in pink. The hydrophobic cleft that is occupied by the Phe42 residue of EZH2 (green sticks) is represented in surface contours. (B) Stabilization of EED mutants by astemizole. The melting curves for 2 μM EED protein in the presence of 200 μM astemizole are shown.

Waals (vdW) and hydrophobic contacts were mediated by the benzyl and 1-ethyl-4-methoxybenzene groups, efficiently anchoring the compound in the EZH2 binding groove (Figure 5). To assess the reliability of the docking model, we used a thermal shift method to characterize the binding of astemizole with distinct EED mutants. As expected, the T_m of wild-type EED was significantly elevated in the presence of astemizole, while no such effect was observed for EED mutants (L246E, L315D, L353A, and F356Y) that harbored mutations in the residues that mediate direct interactions with astemizole in the docking model. Additionally, analogous to the effects observed for wild-type EED, astemizole improved the thermostability of EED proteins with mutations (V112E and L123E) distant from the predicted binding site (Supporting Information Figure S6), supporting the validity of the docking model. However, the individual increases in protein thermostability conferred by astemizole cannot be attributed to the altered thermostability of protein mutants because nearly identical inherent T_m values were observed for the mutants (Supporting Information Figure S7).

dx.doi.org/10.1021/jm501230c | J. Med. Chem. 2014, 57, 9512−9521

To further verify the reliability of the predicted binding mode and explore the essential chemical signature of astemizole that is responsible for its specific binding with EED, we examined the inhibitory activities of its in vivo metabolites.[48] As shown in Supporting Information Figure S8, desmethylastemizole exhibited moderately reduced activity in the FP assay compared with astemizole, which is in agreement with the loss of the hydrophobic interactions between the methyl group and F372 of EED in the docking model. Moreover, significantly impaired inhibitory activity was detected for norastemizole (Supporting Information Figure S8B), which has a much smaller molecular weight from N-dealkylation in vivo.[57] This result could be due to the loss of extensive van der Waals (vdW) and hydrophobic contacts, mediated by 1-ethyl-4-methoxybenzene groups, with the surrounding residues, which is based on the docking simulation (Figure 5A). Nevertheless, the reproducible inhibitory activity of norastemizole in the FP assay, as well as the critical role of the structural elements corresponding to norastemizole in anchoring astemizole at a hydrophobic groove in the PPI interface, indicated that norastemizole may have the core components of astemizole that are required to inhibit the EZH2-EED interaction. We therefore examined the protein-stabilizing effect of norastemizole with the thermal shift assay. Encouragingly, the thermostability of EED was dose-dependently enhanced by norastemizole (Supporting Information Figure S8C), emphasizing the indispensable contributions of the norastemizole scaffold in the disruption of the EZH2-EED complex by astemizole.

CONCLUSIONS AND FUTURE PROSPECTS

The development of potent and selective PRC2 modulators is currently a hot topic of epigenetic drug discovery. Although several EZH2 inhibitors show impressive efficiency in preclinical and clinical studies, the exploration of novel MOAs by targeting EZH2-EED interactions may have broader therapeutic implications for PRC2-addicted human cancers that are either dependent or independent of the HMT activity.[33−35] Additionally, the recent development of highly potent inhibitors targeting the PPI interface, such as WDR5-MLL1,[58,59] Menin-MLL,[60,61] and BRD4-acetyl-lysine complexes,[62,63] has emphasized the validity of epigenetic PPI inhibitors in cancer therapy. It was noteworthy that the PPI inhibitors may gain higher selectivity than the compounds that directly target the active sites of histone modifying enzymes, considering that the allosteric PPI interfaces may have much lower sequence and structural conservation than the enzymatic sites, which is indicated by the recent elegant study on WDR5-MLL1 inhibitors.[58,59] However, no small molecule inhibitors are developed to disrupt the EZH2-EED interactions to date. In the present study, we detailed the identification and characterization of astemizole as a small molecule that can modulate the cellular levels of H3K27me3 modification by disrupting the EZH2-EED interaction of PRC2, an intrinsically difficult PPI target that is characterized by "tight and wide" binding properties.[43] First, a structure-based virtual screening was utilized to identify potential disruptors of the EZH2-EED interactions, from which astemizole was identified as an agent that could displace the EZH2 peptide in the competitive FP assay. Then, multiple lines of biochemical and biophysical evidence demonstrated the unique mechanism of astemizole in impairing the PRC2 activity by directly binding to EED. The cell-based studies further indicated that the dismantling of the EZH2-EED complex by astemizole could efficiently deplete the core components of the PRC2 enzymatic complex, abrogating the PRC2 activities inside cells, which is consistent with the data from both the mutagenesis and RNAi experiments as well as the effects observed for the EZH2 peptide. Moreover, rather than blocking the EAG1 potassium channel, the unique MOA of astemizole disabled the PRC2 complex, which translated into efficient antiproliferation activity in PRC2-driven DLBCLs, confirming the therapeutic potential of the targeted disruption of the EZH2-EED complex as well as providing a novel and complementary strategy for arresting other PRC2-driven human cancers. Last, the molecular modeling studies showed that astemizole was bound to a hydrophobic groove that was occupied by the "hot-spot" residues, providing the putative structural basis for further optimization and helping to identify norastemizole as the core scaffold of astemizole for disrupting the EZH2-EED complex. Because rare, severe cardiotoxicity can occur after astemizole overdose due to the inhibition of the human *ether-a-gogo* related gene (hERG) potassium channel,[64] pharmacologically optimizing astemizole and its minor metabolite norastemizole, which has a much lower activity with potassium channels,[65] will further increase the inhibitory potency against the EZH2-EED complex and diminish the hERG toxicity.

Our findings emphasized the unique MOA of the EZH2-EED PPI disruptors for PRC2 inhibition that the disassociation of the complex accelerated the degradation of PRC2 core components in cells (Figure 2A,B). Therefore, analogous to a chemical reaction equilibrium model, we proposed that the disassociation−association equilibrium of the PRC2 components is largely remodeled by the disruptor of the EZH2-EED interactions in cells (Supporting Information Figure S9). The addition of astemizole irreversibly prompted the degradation of the core components after disassociating EZH2-EED complex, which shifted the equilibrium of PRC2 complex toward a more disassociated state than in vitro. This proposal may account for the better activity of astemizole in the cellular assays. Notably, it could not rule out the possibility that astemizole may bind on other targets as it was a well-known FDA approved drug with histamine H1 antagonist activity, and these effects may also contribute to the cell growth arrest activity. However, the knockdown and target engagement results clearly indicated that astemizole, at least partially, acted on the EZH2-EED interface of the PRC2 complex in cells. More importantly, findings from our present study will lay the foundation for the further development of more potent and selective PRC2 inhibitors for targeted epigenetic therapy, as well as powerful chemical probes in dissecting a variety of Polycomb-related biological pathways.

EXPERIMENTAL SECTION

Virtual Screening and Molecular Docking. An in-house database containing approximately 1000 known drug therapies was screened in silico against the EED structure (PDB entry 2QXV)[49] with the GLIDE 5.5 (grid-based ligand docking with energetics) program.[66,67] The protein structures were prepared using the Protein Preparation Wizard Workflow provided in the Maestro graphical user interface of the Schrödinger program suite, and the default settings were used. Residues within 8 Å around F42 in EZH2 were defined as binding sites in which the docking grids were created. The default settings were adopted for the cutoff, neutralization, scaling, and dimension of the binding pocket. All compounds from the database were docked into the defined binding site without constraint and were ranked based on Glide-score. The top ranking compounds were submitted for further docking validation with the extra precision (XP) mode to eliminate false positives, which was achieved by more

extensive sampling and advanced scoring, resulting in even higher enrichment.[68] Finally, after visual inspection and chemical diversity analysis, the candidate compounds were subjected to the fluorescence polarization assay. In the docking simulation of astemizole against EED, a similar procedure was employed as above.

Protein Expression and Purification. The EED gene (residues 81−441), covering the WD40 repeats,[49] was subcloned into a modified pET28a vector, which contained a SUMO tag after the N-terminal 6 × His tag. The recombinant proteins were overexpressed at 16 °C in *Escherichia coli* strain BL21 (DE3) and then purified by nickel affinity chromatography (GE Healthcare). After removal of His-SUMO tag by ULP1 protease, the elusion was further fractionated by anion-exchange (Mono-Q; GE Healthcare) and size exclusion chromatography (Superdex 75; GE Healthcare). The proteins were concentrated in a buffer containing 25 mM HEPES (pH 8.0), 150 mM NaCl, and 1 mM DTT. A mutated EED construct was made as previously described[69] and the identities were confirmed by sequencing. Mutated proteins were expressed in bacterial cells and purified as above.

Fluorescence Polarization (FP) Assay. Fluorescein-labeled EZH2 helical peptide (residue 39−63) was synthesized on a fully automatic Liberty Blue peptide synthesizer (CEM). In the FP-based binding experiment, serial dilutions of the EED protein were prepared and added into the mixture in 40 μL of FP buffer (25 mM PIPES pH 6.2, 150 mM NaCl, 0.1 mg/mL BSA, and 0.01% NP40) in a 384-well format (Corning 3575). The final concentration of the FITC-labeled peptide was 50 nM and DMSO concentration was 10% (v/v). After incubation at 26 °C for 1 h, the FP was measured on a PerkinElmer EnVision multimode plate reader with an excitation of 485 nm and emission of 520 nm, respectively. The change in the polarization was graphed as a function of the log of the protein concentration, and the apparent dissociation constant (K_d app) was obtained from the sigmoid curve (Supporting Information Figure S1A). After transforming the polarization values (mP) to anisotropy values (mA), the dissociation constant (K_d) was calculated by nonlinearly fitting to eq 1,[70] which is illustrated in Supporting Information Figure S1B.

$$A = A_f + (A_b - A_f) \times \frac{(L_T + K_d + R_T) - \sqrt{(L_T + K_d + R_T)^2 - 4L_T R_T}}{2L_T} \quad (1)$$

Equation employed to calculate the K_d value. A is the experimental anisotropy transformed from the FP values. A_f is the anisotropy for the free ligand and A_b is the anisotropy for the fully bound ligand. L_T and R_T indicate the concentration of the total FITC-labeled peptide and protein. As the anisotropy value (A) is measured for each protein concentration (R_T), the A_b, A_f, and K_d values can be obtained by fitting the data to this equation.

In the FP-based competitive experiment, serial dilutions of competitors for EZH2 were prepared from 100 mM DMSO stocks. The diluted compound was added to the reaction mixture in 40 μL of FP buffer to final concentrations of 0.5 μM EED and 50 nM FITC-labeled peptide. After incubating at 26 °C for 1 h, the FP was measured for each compound concentration and the IC_{50} value was determined using the 4-parameter logistic nonlinear regression model in GraphPad Prism 6. Previous studies have shown quite dramatically how high receptor and labeled ligand concentrations lead to an underestimate of the compound binding affinity from the IC_{50} value.[71−73] We thus turned to exploring the affinity of astemizole to EED by transforming the IC_{50} value to the inhibition constant (K_i), which represents the equilibrium constant of compound binding and theoretically does not depend on the experimental conditions, except the temperature. Then, the mathematical equation (eq 2) or the online K_i calculator (http://sw16.im.med.umich.edu/software/calc_ki/), which were designated for the FP assay by taking into account of the effects from high protein and peptide concentration,[73] was employed to derive the K_i value of astemizole.

$$K_i = \frac{[I]_{50}}{\frac{L_{50}}{K_d} + \frac{[P]_0}{K_d} + 1} \quad (2)$$

The equation used to calculate the K_i value for astemizole. $[I]_{50}$ denotes the concentration of the free inhibitor at 50% inhibition, L_{50} is the concentration of the free labeled ligand at 50% inhibition, $[P]_0$ is the concentration of the free protein at 0% inhibition, and K_d is the dissociation constant of the protein−peptide complex. To obtain the value of $[I]_{50}$, $[P]_0$, and L_{50}, the total concentration of the protein and fluorescence-labeled peptide as well as the dissociation constant of the protein-peptide complex and the IC_{50} value for astemizole were provided.

Thermal Shift Assay. The thermal shift assay was performed on a 7500 fast real-time PCR system (ABI) according to a known protocol.[74,75] Each reaction solution containing 2 μM EED, 5× SYPRO orange (Invitrogen), and testing compounds in 20 μL of thermal shift buffer (25 mM PIPES, pH 6.2, 150 mM NaCl, 1 mM DTT) were heated from 25 to 95 °C at 1% ramp rate. The change in the fluorescence intensities of SYPRO orange was monitored as a function of the temperature. The melting temperature (T_m) was calculated by the Boltzmann fitting method in Protein Thermal Shift Software v 1.1 (ABI). Each reaction was repeated three times.

NMR-Based Binding Assay. Ligand observed T1ρ and saturation transfer difference (STD) NMR experiments were applied to investigate ligand−protein interactions. All NMR spectra were acquired at 25 °C on a Bruker Avance III-600 MHz (proton frequency) spectrometer equipped with a cryogenically cooled probe (Bruker biospin, Germany). Samples containing 400 μM compound, 400 μM compound in the presence of 5 μM protein, and 400 μM compound in the presence of 5 μM protein and 20 μM or 100 μM EZH2 peptide (residues 39−68) were dissolved in phosphate buffer (20 mM NaPO4, 100 mM NaCl, pH 7.4, 10% DMSO) and then used in NMR data acquisition.

In Vitro Histone Methyltransferase (HMT) Assay. Five-component PRC2 holoenzyme (EZH2, SUZ12, EED, RBBP4, and AEBP2) was purchased from Sigma (SRP0134). Enzyme (30 nM) was incubated with an increasing doses of the inhibitor (i.e., 10 nM, 100 nM, 1 μM, 10 μM, and 100 μM) in the presence of 5% DMSO on ice for 30 min. Histone octamer (454 nM) and 48 μM SAM were subsequently added and the reaction was carried out in a buffer containing 25 mM Tris-HCl, pH 8.0, 10 mM NaCl, 1 mM EDTA, 2.5 mM MgCl2, 1 mM DTT, 5% Glycerol, and 2% DMSO at 30 °C for 4 h. The reaction was stopped by 1× SDS loading dye and the product was resolved by SDS-PAGE. The H3K27me3 signal was detected by an anti-H3K27me3 antibody from Abcam (ab6002).

Western Blot Analysis. To detected PRC2 component degradation and H3K27me3 reduction, DB and Toledo cells were treated with astemizole or doxorubicin for 72 h. Then, the cells were lysed with RIPA buffer (50 mM Tris-HCl pH 8.0; 150 mM NaCl; 1% NP-40; 0.5% sodium deoxycholate; and 0.1% SDS). Lysates with 30 μg of total protein were separated with SDS-PAGE, and transferred to a PVDF membrane (GE Healthcare). The blots were probed with the indicated primary antibodies followed by HRP-conjugated anti-rabbit or anti-mouse IgG antibody. Detection was performed with chemiluminescent HRP substrate (GE Healthcare). For immunoblot against other histone H3 methylation modifications, samples were prepared as described.[27]

Cell Viability Analysis. Diffused large B-cell lymphoma cell lines (SU-DHL6, Toledo, DB, SU-DHL4, and Pfeiffer) were obtained from American Type Culture Collection (ATCC, Manassas, VA) and cultured in RPMI 1640 medium supplemented with 10% FBS and 1 × Pen/Strep. To determine the effect of astemizole on DLBCL cells, the cells (1−2 × 10^4 cells per well) were placed in 100 μL of serum-containing media with astemizole in 96-well flat-bottomed microtiter plates in triplicate cultures. The cell viability was measured by Cell Counting Kit-8 (CCK8, Dojindo) after 7 days incubation. The absorbance was measured at a 450 nm with 600 nm as the reference using a microculture plate reader (POLARstar Omega, Offenburg). The cell viability was expressed as the percentage of absorbance in cells

with indicated treatments to that in the control cells. To determine the effect of astemizole on both the shEED and shEZH2 treated DB cells, the cells (5000 cells per well) were placed in 200 μL of serum-containing media with astemizole in 96-well flat-bottomed microtiter plates in triplicate cultures. The cell viability was measured by alamar blue assay after 3 days incubation. Following the addition of 20 μL of alamar blue (Invitrogen), the plates were incubated at 37 °C and read at 560 nm.

Flow Cytometry Assay. Cell apoptosis was determined by dual staining with annexin V conjugated to FITC and 7-amino-actinomycin (7AAD). DB and Toledo cells were treated with 0, 0.6, 1.25, 2.5, 5, and 10 μM astemizole for 72 h. Then, according to the protocol, 1×10^6 cells were stained with annexin V-FITC and 7AAD (Annexin V FITC apoptosis detection kit I, BD Pharmingen) for 15 min in the dark and analyzed by flow cytometry using a FACS Calibur cytometer (BD Pharmingen). To evaluate the effects of combination treatment at the indicated dose of astemizole and EPZ in DB and Toledo cells, DB and Toledo cells were treated with EPZ and/or astemizole for 72 h, and the cell viability was measured by flow cytometry as described above. Apoptotic cells were identified as annexin V^+ and/or $7AAD^+$ cells. Cells excluding both annexin V-FITC and 7AAD were considered viable.

RNAi Plasmid. Primers of shRNA-Mock (Mock), shRNA-EED (shEED), or shRNA-EZH2 (shEZH2) were designed and cloned into the lentiviral pSICOR vector, respectively. Lentiviruses were produced in HEK239T cells, maintained in 1640 supplemented with 10% FBS without antibiotic, byco-transfecting pSicoR, psPAX2, and pMD2.G with lipofectamine 2000 (Invitrogen). Culture supernatants containing pseudotyped lentiviral particles were filtered by 0.22 μm filter (Millipore). Primers for Mock, EED, and EZH2 shRNA were as follows: shRNA-Mock (sh-Mock): GGAACCGTCTTGCAGTA-CATTT; shRNA-EED (shEED): GCCAGTGTGACATTTGGTAT-3′; and shRNA-EZH2 (shEZH2): 5′-GCTCTAGACAACAAACC-TTT-3′, respectively.

Source and Purity of Astemizole. Astemizole was purchased from the Sigma-Aldrich company (A2861), who claimed to have more than 98% purity of the compound based on a high performance liquid chromatography (HPLC) analysis.

■ ASSOCIATED CONTENT

Ⓢ Supporting Information

Experimental details to derive the K_i value in the FP assay, ligand observed STD spectrum, in vitro histone methyltransferase (HMT) assay, MOA comparison with doxorubicin, drug combination, cell viability analysis, and thermostability of EED mutants. This material is available free of charge via the Internet at http://pubs.acs.org.

■ AUTHOR INFORMATION

Corresponding Author

*Telephone: 86-21-50806600. E-mail: cluo@simm.ac.cn.

Author Contributions

‡Xiangqian Kong and Limin Chen contributed equally.

Notes

The authors declare no competing financial interest.

■ ACKNOWLEDGMENTS

We thank Dr. Yongjun Dang from Fudan University for helpful discussion for this study. The computation resources were supported by Computer Network Information Center, Chinese Academy of Sciences and Shanghai Supercomputing Center. This work was supported by the Hi-Tech Research and Development Program of China (2012AA020302 to C.L.), the National Natural Science Foundation of China (21210003 and 81230076 to H.J., 91229204 to C.L. and 21272246 to N.Z.), the National Science and Technology Major Project "Key New Drug Creation and Manufacturing Program" (2014ZX09507002 to C.L.), Chinese Academy of Sciences grants (100 Talents Program to N.Z.), and the Welch Foundation research grant (I-1790) to X.L.

■ ABBREVIATIONS

FDA, Food and Drug Administration; EZH2, enhancer of zeste homologue 2; EED, embryonic ectoderm development; SUZ12, suppressor of zeste 12 homologue; RT-PCR, reverse transcription polymerase chain reaction; shRNA, short hairpin RNA; WDR5, WD repeat-containing protein 5; MLL1, myeloid/lymphoid, or mixed-lineage, leukemia 1; Menin, multiple endocrine neoplasia I; BRD4, bromodomain-containing protein 4

■ REFERENCES

(1) Berger, S. L. The complex language of chromatin regulation during transcription. *Nature* **2007**, *447*, 407−412.

(2) Kouzarides, T. Chromatin modifications and their function. *Cell* **2007**, *128*, 693−705.

(3) Rice, J. C.; Briggs, S. D.; Ueberheide, B.; Barber, C. M.; Shabanowitz, J.; Hunt, D. F.; Shinkai, Y.; Allis, C. D. Histone methyltransferases direct different degrees of methylation to define distinct chromatin domains. *Mol. Cell* **2003**, *12*, 1591−1598.

(4) Zhang, Y.; Reinberg, D. Transcription regulation by histone methylation: interplay between different covalent modifications of the core histone tails. *Genes Dev.* **2001**, *15*, 2343−2360.

(5) Izzo, A.; Schneider, R. Chatting histone modifications in mammals. *Briefings in Functional Genomics* **2010**, *9*, 429−443.

(6) Greer, E. L.; Shi, Y. Histone methylation: a dynamic mark in health, disease and inheritance. *Nat. Rev. Genet.* **2012**, *13*, 343−357.

(7) Wagner, T.; Jung, M. New lysine methyltransferase drug targets in cancer. *Nat. Biotechnol.* **2012**, *30*, 622−623.

(8) Copeland, R. A.; Solomon, M. E.; Richon, V. M. Protein methyltransferases as a target class for drug discovery. *Nat. Rev. Drug Discovery* **2009**, *8*, 724−732.

(9) Lewis, E. B. A gene complex controlling segmentation in Drosophila. *Nature* **1978**, *276*, 565−570.

(10) Margueron, R.; Reinberg, D. The Polycomb complex PRC2 and its mark in life. *Nature* **2011**, *469*, 343−349.

(11) Schuettengruber, B.; Cavalli, G. Recruitment of Polycomb group complexes and their role in the dynamic regulation of cell fate choice. *Development* **2009**, *136*, 3531−3542.

(12) Zhou, W.; Zhu, P.; Wang, J.; Pascual, G.; Ohgi, K. A.; Lozach, J.; Glass, C. K.; Rosenfeld, M. G. Histone H2A monoubiquitination represses transcription by inhibiting RNA polymerase II transcriptional elongation. *Mol. Cell* **2008**, *29*, 69−80.

(13) Stock, J. K.; Giadrossi, S.; Casanova, M.; Brookes, E.; Vidal, M.; Koseki, H.; Brockdorff, N.; Fisher, A. G.; Pombo, A. Ring1-mediated ubiquitination of H2A restrains poised RNA polymerase II at bivalent genes in mouse ES cells. *Nat. Cell Biol.* **2007**, *9*, 1428−1435.

(14) Sparmann, A.; van Lohuizen, M. Polycomb silencers control cell fate, development and cancer. *Nat. Rev. Cancer* **2006**, *6*, 846−856.

(15) Whitcomb, S. J.; Basu, A.; Allis, C. D.; Bernstein, E. Polycomb Group proteins: an evolutionary perspective. *Trends Genet.* **2007**, *23*, 494−502.

(16) Simon, J. A.; Kingston, R. E. Mechanisms of polycomb gene silencing: knowns and unknowns. *Nat. Rev. Mol. Cell Biol.* **2009**, *10*, 697−708.

(17) Czermin, B.; Melfi, R.; McCabe, D.; Seitz, V.; Imhof, A.; Pirrotta, V. Drosophila enhancer of Zeste/ESC complexes have a histone H3 methyltransferase activity that marks chromosomal polycomb sites. *Cell* **2002**, *111*, 185−196.

(18) Cao, R.; Zhang, Y. SUZ12 is required for both the histone methyltransferase activity and the silencing function of the EED-EZH2 complex. *Mol. Cell* **2004**, *15*, 57−67.

(19) Chang, C. J.; Hung, M. C. The role of EZH2 in tumour progression. *Br. J. Cancer* **2012**, *106*, 243−247.
(20) Chase, A.; Cross, N. C. Aberrations of EZH2 in cancer. *Clin. Cancer Res.* **2011**, *17*, 2613−2618.
(21) Morin, R. D.; Johnson, N. A.; Severson, T. M.; Mungall, A. J.; An, J.; Goya, R.; Paul, J. E.; Boyle, M.; Woolcock, B. W.; Kuchenbauer, F.; Yap, D.; Humphries, R. K.; Griffith, O. L.; Shah, S.; Zhu, H.; Kimbara, M.; Shashkin, P.; Charlot, J. F.; Tcherpakov, M.; Corbett, R.; Tam, A.; Varhol, R.; Smailus, D.; Moksa, M.; Zhao, Y.; Delaney, A.; Qian, H.; Birol, I.; Schein, J.; Moore, R.; Holt, R.; Horsman, D. E.; Connors, J. M.; Jones, S.; Aparicio, S.; Hirst, M.; Gascoyne, R. D.; Marra, M. A. Somatic mutations altering EZH2 (Tyr641) in follicular and diffuse large B-cell lymphomas of germinal-center origin. *Nat. Genet.* **2010**, *42*, 181−185.
(22) Yap, D. B.; Chu, J.; Berg, T.; Schapira, M.; Cheng, S. W. G.; Moradian, A.; Morin, R. D.; Mungall, A. J.; Meissner, B.; Boyle, M.; Marquez, V. E.; Marra, M. A.; Gascoyne, R. D.; Humphries, R. K.; Arrowsmith, C. H.; Morin, G. B.; Aparicio, S. A. J. R. Somatic mutations at EZH2 Y641 act dominantly through a mechanism of selectively altered PRC2 catalytic activity, to increase H3K27 trimethylation. *Blood* **2011**, *117*, 2451−2459.
(23) Sneeringer, C. J.; Scott, M. P.; Kuntz, K. W.; Knutson, S. K.; Pollock, R. M.; Richon, V. M.; Copeland, R. A. Coordinated activities of wild-type plus mutant EZH2 drive tumor-associated hyper-trimethylation of lysine 27 on histone H3 (H3K27) in human B-cell lymphomas. *Proc. Natl. Acad. Sci. U. S. A.* **2010**, *107*, 20980−20985.
(24) Beguelin, W.; Popovic, R.; Teater, M.; Jiang, Y. W.; Bunting, K. L.; Rosen, M.; Shen, H.; Yang, S. N.; Wang, L.; Ezponda, T.; Martinez-Garcia, E.; Zhang, H. K.; Zheng, Y. P.; Verma, S. K.; McCabe, M. T.; Ott, H. M.; Van Aller, G. S.; Kruger, R. G.; Liu, Y.; McHugh, C. F.; Scott, D. W.; Chung, Y. R.; Kelleher, N.; Shaknovich, R.; Creasy, C. L.; Gascoyne, R. D.; Wong, K. K.; Cerchietti, L.; Levine, R. L.; Abdel-Wahab, O.; Licht, J. D.; Elemento, O.; Melnick, A. M. EZH2 is required for germinal center formation and somatic EZH2 mutations promote lymphoid transformation. *Cancer Cell* **2013**, *23*, 677−692.
(25) Knutson, S. K.; Wigle, T. J.; Warholic, N. M.; Sneeringer, C. J.; Allain, C. J.; Klaus, C. R.; Sacks, J. D.; Raimondi, A.; Majer, C. R.; Song, J.; Scott, M. P.; Jin, L.; Smith, J. J.; Olhava, E. J.; Chesworth, R.; Moyer, M. P.; Richon, V. M.; Copeland, R. A.; Keilhack, H.; Pollock, R. M.; Kuntz, K. W. A selective inhibitor of EZH2 blocks H3K27 methylation and kills mutant lymphoma cells. *Nat. Chem. Biol.* **2012**, *8*, 890−896.
(26) McCabe, M. T.; Ott, H. M.; Ganji, G.; Korenchuk, S.; Thompson, C.; Van Aller, G. S.; Liu, Y.; Graves, A. P.; Della Pietra, A.; Diaz, E.; LaFrance, L. V.; Mellinger, M.; Duquenne, C.; Tian, X. R.; Kruger, R. G.; McHugh, C. F.; Brandt, M.; Miller, W. H.; Dhanak, D.; Verma, S. K.; Tummino, P. J.; Creasy, C. L. EZH2 inhibition as a therapeutic strategy for lymphoma with EZH2-activating mutations. *Nature* **2012**, *492*, 108−102.
(27) Qi, W.; Chan, H. M.; Teng, L.; Li, L.; Chuai, S. N.; Zhang, R. P.; Zeng, J.; Li, M.; Fan, H.; Lin, Y.; Gu, J.; Ardayfio, O.; Zhang, J. H.; Yan, X. X.; Fang, J. L.; Mi, Y.; Zhang, M.; Zhou, T.; Feng, G.; Chen, Z. J.; Li, G. B.; Yang, T.; Zhao, K. H.; Liu, X. H.; Yu, Z. T.; Lu, C. X.; Atadja, P.; Li, E. Selective inhibition of Ezh2 by a small molecule inhibitor blocks tumor cells proliferation. *Proc. Natl. Acad. Sci. U.S.A.* **2012**, *109*, 21360−21365.
(28) Denisenko, O.; Shnyreva, M.; Suzuki, H.; Bomsztyk, K. Point mutations in the WD40 domain of Eed block its interaction with Ezh2. *Mol. Cell. Biol.* **1998**, *18*, 5634−5642.
(29) Cao, R.; Wang, L.; Wang, H.; Xia, L.; Erdjument-Bromage, H.; Tempst, P.; Jones, R. S.; Zhang, Y. Role of histone H3 lysine 27 methylation in Polycomb-group silencing. *Science* **2002**, *298*, 1039−1043.
(30) Montgomery, N. D.; Yee, D.; Montgomery, S. A.; Magnuson, T. Molecular and functional mapping of EED motifs required for PRC2-dependent histone methylation. *J. Mol. Biol.* **2007**, *374*, 1145−1157.
(31) Montgomery, N. D.; Yee, D.; Chen, A.; Kalantry, S.; Chamberlain, S. J.; Otte, A. P.; Magnuson, T. The murine polycomb group protein Eed is required for global histone H3 lysine-27 methylation. *Curr. Biol.* **2005**, *15*, 942−947.
(32) Kim, W.; Bird, G. H.; Neff, T.; Guo, G.; Kerenyi, M. A.; Walensky, L. D.; Orkin, S. H. Targeted disruption of the EZH2-EED complex inhibits EZH2-dependent cancer. *Nat. Chem. Biol.* **2013**, *9*, 643−650.
(33) Lee, S. T.; Li, Z.; Wu, Z.; Aau, M.; Guan, P.; Karuturi, R. K.; Liou, Y. C.; Yu, Q. Context-specific regulation of NF-kappaB target gene expression by EZH2 in breast cancers. *Mol. Cell* **2011**, *43*, 798−810.
(34) Xu, K.; Wu, Z. J.; Groner, A. C.; He, H. H.; Cai, C.; Lis, R. T.; Wu, X.; Stack, E. C.; Loda, M.; Liu, T.; Xu, H.; Cato, L.; Thornton, J. E.; Gregory, R. I.; Morrissey, C.; Vessella, R. L.; Montironi, R.; Magi-Galluzzi, C.; Kantoff, P. W.; Balk, S. P.; Liu, X. S.; Brown, M. EZH2 oncogenic activity in castration-resistant prostate cancer cells is Polycomb-independent. *Science* **2012**, *338*, 1465−1469.
(35) Wee, Z. N.; Li, Z.; Lee, P. L.; Lee, S. T.; Lim, Y. P.; Yu, Q. EZH2-mediated inactivation of IFN-gamma-JAK-STAT1 signaling is an effective therapeutic target in MYC-driven prostate cancer. *Cell Rep.* **2014**, *8*, 204−216.
(36) Zinzalla, G.; Thurston, D. E. Targeting protein-protein interactions for therapeutic intervention: a challenge for the future. *Future Med. Chem.* **2009**, *1*, 65−93.
(37) Arkin, M. R.; Wells, J. A. Small-molecule inhibitors of protein-protein interactions: progressing towards the dream. *Nat. Rev. Drug Discovery* **2004**, *3*, 301−317.
(38) Shangary, S.; Wang, S. Small-molecule inhibitors of the MDM2-p53 protein-protein interaction to reactivate p53 function: a novel approach for cancer therapy. *Annu. Rev. Pharmacol. Toxicol.* **2009**, *49*, 223−241.
(39) Zhou, H.; Aguilar, A.; Chen, J.; Bai, L.; Liu, L.; Meagher, J. L.; Yang, C. Y.; McEachern, D.; Cong, X.; Stuckey, J. A.; Wang, S. Structure-based design of potent Bcl-2/Bcl-xL inhibitors with strong in vivo antitumor activity. *J. Med. Chem.* **2012**, *55*, 6149−6161.
(40) Zhao, Y.; Yu, S.; Sun, W.; Liu, L.; Lu, J.; McEachern, D.; Shargary, S.; Bernard, D.; Li, X.; Zhao, T.; Zou, P.; Sun, D.; Wang, S. A potent small-molecule inhibitor of the MDM2-p53 interaction (MI-888) achieved complete and durable tumor regression in mice. *J. Med. Chem.* **2013**, *56*, 5553−5561.
(41) Sun, H.; Lu, J.; Liu, L.; Yi, H.; Qiu, S.; Yang, C. Y.; Deschamps, J. R.; Wang, S. Nonpeptidic and potent small-molecule inhibitors of cIAP-1/2 and XIAP proteins. *J. Med. Chem.* **2010**, *53*, 6361−6367.
(42) Mullard, A. Protein-protein interaction inhibitors get into the groove. *Nat. Rev. Drug Discovery* **2012**, *11*, 172−174.
(43) Smith, M. C.; Gestwicki, J. E. Features of protein-protein interactions that translate into potent inhibitors: topology, surface area and affinity. *Expert Reviews in Molecular Medicine* **2012**, *14*, e16.
(44) Lu, Y.; Nikolovska-Coleska, Z.; Fang, X.; Gao, W.; Shangary, S.; Qiu, S.; Qin, D.; Wang, S. Discovery of a nanomolar inhibitor of the human murine double minute 2 (MDM2)-p53 interaction through an integrated, virtual database screening strategy. *J. Med. Chem.* **2006**, *49*, 3759−3762.
(45) Kong, X. Q.; Qin, J.; Li, Z.; Vultur, A.; Tong, L. J.; Feng, E. G.; Rajan, G.; Liu, S. E.; Lu, J. Y.; Liang, Z. J.; Zheng, M. Y.; Zhu, W. L.; Jiang, H. L.; Herlyn, M.; Liu, H.; Marmorstein, R.; Luo, C. Development of a novel class of B-Raf(V600E)-selective inhibitors through virtual screening and hierarchical hit optimization. *Org. Biomol. Chem.* **2012**, *10*, 7402−7417.
(46) Carlsson, J.; Coleman, R. G.; Setola, V.; Irwin, J. J.; Fan, H.; Schlessinger, A.; Sali, A.; Roth, B. L.; Shoichet, B. K. Ligand discovery from a dopamine D3 receptor homology model and crystal structure. *Nat. Chem. Biol.* **2011**, *7*, 769−778.
(47) London, N.; Miller, R. M.; Krishnan, S.; Uchida, K.; Irwin, J. J.; Eidam, O.; Gibold, L.; Cimermancic, P.; Bonnet, R.; Shoichet, B. K.; Taunton, J. Covalent docking of large libraries for the discovery of chemical probes. *Nat. Chem. Biol.* [Online Early Access] DOI: 10.1038/nchembio.1666; Published Online Oct 26, **2014**
(48) Janssens, M. M. Astemizole. A nonsedating antihistamine with fast and sustained activity. *Clin. Rev. Allergy* **1993**, *11*, 35−63.

(49) Han, Z.; Xing, X.; Hu, M.; Zhang, Y.; Liu, P.; Chai, J. Structural basis of EZH2 recognition by EED. *Structure* **2007**, *15*, 1306−1315.
(50) Wendel, H. G.; De Stanchina, E.; Fridman, J. S.; Malina, A.; Ray, S.; Kogan, S.; Cordon-Cardo, C.; Pelletier, J.; Lowe, S. W. Survival signalling by Akt and eIF4E in oncogenesis and cancer therapy. *Nature* **2004**, *428*, 332−337.
(51) Garcia-Quiroz, J.; Camacho, J. Astemizole: an old anti-histamine as a new promising anti-cancer drug. *Anti-Cancer Agents in Medicinal Chemistry* **2011**, *11*, 307−314.
(52) Garcia-Ferreiro, R. E.; Kerschensteiner, D.; Major, F.; Monje, F.; Stuhmer, W.; Pardo, L. A. Mechanism of block of hEag1 K+ channels by imipramine and astemizole. *J. Gen. Physiol.* **2004**, *124*, 301−317.
(53) Diaz, L.; Ceja-Ochoa, I.; Restrepo-Angulo, I.; Larrea, F.; Avila-Chavez, E.; Garcia-Becerra, R.; Borja-Cacho, E.; Barrera, D.; Ahumada, E.; Gariglio, P.; Alvarez-Rios, E.; Ocadiz-Delgado, R.; Garcia-Villa, E.; Hernandez-Gallegos, E.; Camacho-Arroyo, I.; Morales, A.; Ordaz-Rosado, D.; Garcia-Latorre, E.; Escamilla, J.; Sanchez-Pena, L. C.; Saqui-Salces, M.; Gamboa-Dominguez, A.; Vera, E.; Uribe-Ramirez, M.; Murbartian, J.; Ortiz, C. S.; Rivera-Guevara, C.; De Vizcaya-Ruiz, A.; Camacho, J. Estrogens and human papilloma virus oncogenes regulate human ether-a-go-go-1 potassium channel expression. *Cancer Res.* **2009**, *69*, 3300−3307.
(54) Restrepo-Angulo, I.; Sanchez-Torres, C.; Camacho, J. Human EAG1 potassium channels in the epithelial-to-mesenchymal transition in lung cancer cells. *Anticancer Res.* **2011**, *31*, 1265−1270.
(55) Borowiec, A. S.; Hague, F.; Harir, N.; Guenin, S.; Guerineau, F.; Gouilleux, F.; Roudbaraki, M.; Lassoued, K.; Ouadid-Ahidouch, H. IGF-1 activates hEAG K(+) channels through an Akt-dependent signaling pathway in breast cancer cells: role in cell proliferation. *J. Cell Physiol.*. **2007**, *212*, 690−701.
(56) Roy, J.; Vantol, B.; Cowley, E. A.; Blay, J.; Linsdell, P. Pharmacological separation of hEAG and hERG K+ channel function in the human mammary carcinoma cell line MCF-7. *Oncol. Rep.* **2008**, *19*, 1511−1516.
(57) Matsumoto, S.; Yamazoe, Y. Involvement of multiple human cytochromes P450 in the liver microsomal metabolism of astemizole and a comparison with terfenadine. *Br. J. Clin. Pharmacol.* **2001**, *51*, 133−142.
(58) Karatas, H.; Townsend, E. C.; Cao, F.; Chen, Y.; Bernard, D.; Liu, L.; Lei, M.; Dou, Y.; Wang, S. High-affinity, small-molecule peptidomimetic inhibitors of MLL1/WDR5 protein-protein interaction. *J. Am. Chem. Soc.* **2013**, *135*, 669−682.
(59) Cao, F.; Townsend, E. C.; Karatas, H.; Xu, J.; Li, L.; Lee, S.; Liu, L.; Chen, Y.; Ouillette, P.; Zhu, J.; Hess, J. L.; Atadja, P.; Lei, M.; Qin, Z. S.; Malek, S.; Wang, S.; Dou, Y. Targeting MLL1 H3K4 methyltransferase activity in mixed-lineage leukemia. *Mol. Cell* **2014**, *53*, 247−261.
(60) Zhou, H.; Liu, L.; Huang, J.; Bernard, D.; Karatas, H.; Navarro, A.; Lei, M.; Wang, S. Structure-based design of high-affinity macrocyclic peptidomimetics to block the menin-mixed lineage leukemia 1 (MLL1) protein-protein interaction. *J. Med. Chem.* **2013**, *56*, 1113−1123.
(61) Grembecka, J.; He, S.; Shi, A.; Purohit, T.; Muntean, A. G.; Sorenson, R. J.; Showalter, H. D.; Murai, M. J.; Belcher, A. M.; Hartley, T.; Hess, J. L.; Cierpicki, T. Menin-MLL inhibitors reverse oncogenic activity of MLL fusion proteins in leukemia. *Nat. Chem. Biol.* **2012**, *8*, 277−84.
(62) Delmore, J. E.; Issa, G. C.; Lemieux, M. E.; Rahl, P. B.; Shi, J. W.; Jacobs, H. M.; Kastritis, E.; Gilpatrick, T.; Paranal, R. M.; Qi, J.; Chesi, M.; Schinzel, A. C.; McKeown, M. R.; Heffernan, T. P.; Vakoc, C. R.; Bergsagel, P. L.; Ghobrial, I. M.; Richardson, P. G.; Young, R. A.; Hahn, W. C.; Anderson, K. C.; Kung, A. L.; Bradner, J. E.; Mitsiades, C. S. BET bromodomain inhibition as a therapeutic strategy to target c-Myc. *Cell* **2011**, *146*, 903−916.
(63) Asangani, I. A.; Dommeti, V. L.; Wang, X.; Malik, R.; Cieslik, M.; Yang, R.; Escara-Wilke, J.; Wilder-Romans, K.; Dhanireddy, S.; Engelke, C.; Iyer, M. K.; Jing, X.; Wu, Y. M.; Cao, X.; Qin, Z. S.; Wang, S.; Feng, F. Y.; Chinnaiyan, A. M. Therapeutic targeting of BET bromodomain proteins in castration-resistant prostate cancer. *Nature* **2014**, *510*, 278−282.
(64) Zhou, S. F.; Chan, S. Y.; Goh, B. C.; Chan, E.; Duan, W.; Huang, M.; McLeod, H. L. Mechanism-based inhibition of cytochrome P450 3A4 by therapeutic drugs. *Clinical Pharmacokinetics* **2005**, *44*, 279−304.
(65) Zhou, Z.; Vorperian, V. R.; Gong, Q.; Zhang, S.; January, C. T. Block of HERG potassium channels by the antihistamine astemizole and its metabolites desmethylastemizole and norastemizole. *J. Cardiovasc. Electrophysiol.* **1999**, *10*, 836−843.
(66) Friesner, R. A.; Banks, J. L.; Murphy, R. B.; Halgren, T. A.; Klicic, J. J.; Mainz, D. T.; Repasky, M. P.; Knoll, E. H.; Shelley, M.; Perry, J. K.; Shaw, D. E.; Francis, P.; Shenkin, P. S. Glide: a new approach for rapid, accurate docking and scoring. 1. Method and assessment of docking accuracy. *J. Med. Chem.* **2004**, *47*, 1739−1749.
(67) Halgren, T. A.; Murphy, R. B.; Friesner, R. A.; Beard, H. S.; Frye, L. L.; Pollard, W. T.; Banks, J. L. Glide: a new approach for rapid, accurate docking and scoring. 2. Enrichment factors in database screening. *J. Med. Chem.* **2004**, *47*, 1750−1759.
(68) Friesner, R. A.; Murphy, R. B.; Repasky, M. P.; Frye, L. L.; Greenwood, J. R.; Halgren, T. A.; Sanschagrin, P. C.; Mainz, D. T. Extra precision glide: docking and scoring incorporating a model of hydrophobic enclosure for protein-ligand complexes. *J. Med. Chem.* **2006**, *49*, 6177−96.
(69) Xu, C.; Bian, C.; Yang, W.; Galka, M.; Ouyang, H.; Chen, C.; Qiu, W.; Liu, H.; Jones, A. E.; MacKenzie, F.; Pan, P.; Li, S. S.; Wang, H.; Min, J. Binding of different histone marks differentially regulates the activity and specificity of polycomb repressive complex 2 (PRC2). *Proc. Natl. Acad. Sci. U. S. A.* **2010**, *107*, 19266−19271.
(70) Lundblad, J. R.; Laurance, M.; Goodman, R. H. Fluorescence polarization analysis of protein-DNA and protein-protein interactions. *Mol. Endocrinol.* **1996**, *10*, 607−612.
(71) Munson, P. J.; Rodbard, D. An exact correction to the ″Cheng-Prusoff″ correction. *J. Recept. Res.* **1988**, *8*, 533−546.
(72) Swillens, S. Interpretation of binding curves obtained with high receptor concentrations - practical aid for computer-analysis. *Mol. Pharmacol.* **1995**, *47*, 1197−1203.
(73) Nikolovska-Coleska, Z.; Wang, R. X.; Fang, X. L.; Pan, H. G.; Tomita, Y.; Li, P.; Roller, P. P.; Krajewski, K.; Saito, N. G.; Stuckey, J. A.; Wang, S. M. Development and optimization of a binding assay for the XIAP BIR3 domain using fluorescence polarization. *Anal. Biochem.* **2004**, *332*, 261−273.
(74) Niesen, F. H.; Berglund, H.; Vedadi, M. The use of differential scanning fluorimetry to detect ligand interactions that promote protein stability. *Nat. Protoc.* **2007**, *2*, 2212−2221.
(75) Chen, B.; Ye, F.; Yu, L.; Jia, G.; Huang, X.; Zhang, X.; Peng, S.; Chen, K.; Wang, M.; Gong, S.; Zhang, R.; Yin, J.; Li, H.; Yang, Y.; Liu, H.; Zhang, J.; Zhang, H.; Zhang, A.; Jiang, H.; Luo, C.; Yang, C. G. Development of cell-active N6-methyladenosine RNA demethylase FTO inhibitor. *J. Am. Chem. Soc.* **2012**, *134*, 17963−17971.